

A TOMOGRAPHIC FRAMEWORK FOR LIDAR IMAGING

Peter J. Shargo, Nail Çadallı, Andrew C. Singer, David C. Munson, Jr.

Coordinated Science Laboratory and Department of Electrical and Computer Engineering
University of Illinois at Urbana-Champaign, 1308 West Main Street, Urbana, IL 61801
{shargo,cadalli,acsinger,d-munson}@uiuc.edu

ABSTRACT

Detection and localization of underwater mines remains a challenging and important problem for safe operation of naval platforms. A number of new technologies exploit airborne LIDARs, which can penetrate the air-water interface and optically detect and localize underwater mines. Such systems process the received optical field generated by scattering within the water column, and have proven to be an effective technology for mine detection and localization. In this work, we consider the use of multiple looks at a single target to form a three-dimensional representation of the scatterers within the water column. To form such images, we account for the integration within the receive sensors, and formulate the problem in a tomographic framework. We will present preliminary image formation results generated from data collected at sea with a state-of-the-art Navy mine imaging system.

1. INTRODUCTION

Airborne LIDAR (light detection and ranging) systems are effective at detecting and localizing underwater objects such as mines and submarines. This is typically done by capturing parts of the reflected optical field with sensors such as CCDs (charge coupled devices) and PMTs (photomultiplier tubes). The CCDs generate images of the scatterers in the illuminated water column, while the PMT returns provide information about the scene in the range direction. The images and PMT returns are analyzed and processed to accurately determine which objects are likely mines, and where they are located. In this paper, we work with a data set from a previous study (1998 Competitive Evaluation Field Test (CEFT)) collected by a system designed for the detection and localization problem. We extend this application to a three dimensional tomographic reconstruction problem. Our data set consists of CCD images and PMT returns from scenes containing the same mine at different times and angular orientations; thus, each gives different information about the size and shape of the object. We show that, by treating these CCD images and PMT returns as projections, 3D reconstructions of the mine can be obtained whose quality depends mostly on the angular diversity of the projections. First, we discuss the nature of the collected CEFT data. Second, we present a tomographic framework, and discuss how the CCD images and PMT returns can be treated within this framework. Third, we discuss our algorithm for the reconstruction of 3D objects from this data. Finally, we present our preliminary results, including reconstructions from both the real data and theoretical projections of a spherical object.

This work was supported by the Office of Naval Research under grant N61331-00-1-G001.

2. CEFT DATA

The collected CEFT data consists of CCD images and time resolved PMT returns from an airborne LIDAR system flying approximately 360 meters above the ocean surface. The LIDAR system used a 100 mJ pulsed laser at a wavelength of 532 nm, firing several pulses per second, with each pulse of duration 6 ns. The two types of sensors, CCD and PMT, each collected data from every pulse as it was scattered back to the optics from objects within the water column. For each pulse, a 64×64 pixel CCD image and five PMT returns sampled at 6 ns were collected. Each PMT channel served a different function; one was used to detect the surface of the water, while each of the other four was focused on a different quadrant of the laser spot on the water surface; that is, each quadrant in the resulting CCD image has its own respective photomultiplier tube measuring photons from roughly the same particular volume of water. If a mine is seen in a particular quadrant of the CCD image, we expect to see evidence of the mine in the PMT focused on that same quadrant, and vice versa. Each PMT is able to collect photons from a large fraction of the illuminated water volume, and can therefore be sampled sufficiently fast to obtain precise range information. However, since the PMT is optically boresighted to a wide area of the illuminated water column, little spatial information is collected beyond the simple 2×2 PMT pixel array. On the other hand, the CCD image is collected by gating the return around a particular range of depths in the water column. This gate must be large (deep) enough to ensure that a target return from a reflected mine will be completely captured (integrated). However, if it is too large, the signal will be overwhelmed by the background scatterers in the medium. The particular mine which was reconstructed has a true diameter of 1 m, and appears on the CCD with a width of approximately 6 to 7 pixels.

3. TOMOGRAPHIC FRAMEWORK

Given a 3D object that exhibits a property g defined in three space by $g(x_1, x_2, x_3)$, we define the following linear projection $p_1(x_3)$:

$$p_1(x_3) = \iint_{-\infty}^{\infty} g(x_1, x_2, x_3) dx_1 dx_2.$$

Similarly, we can also define a planar projection $p_2(x_1, x_2)$:

$$p_2(x_1, x_2) = \int_{-\infty}^{\infty} g(x_1, x_2, x_3) dx_3.$$

Thus, the former projection maps the function $g(x_1, x_2, x_3)$ onto a one dimensional function $p_1(x_3)$ by integrating across planes,

while the latter projection maps $g(x_1, x_2, x_3)$ onto a two dimensional function $p_2(x_1, x_2)$ through line integrals.

The Projection-Slice Theorem [1, 2] demonstrates the following relationships between the Fourier transform $G(\omega_1, \omega_2, \omega_3)$ of $g(x_1, x_2, x_3)$ and the Fourier transforms of its projections:

$$\begin{aligned} P_1(\omega_3) &= \int_{-\infty}^{\infty} p_1(x_3) e^{-j\omega_3 x_3} d\omega_3 \\ &= \iiint_{-\infty}^{\infty} g(x_1, x_2, x_3) e^{-j\omega_3 x_3} dx_1 dx_2 dx_3 \\ &= G(\omega_1, \omega_2, \omega_3) |_{\omega_1=\omega_2=0} \\ &= G(0, 0, \omega_3). \end{aligned} \quad (1)$$

$$\begin{aligned} P_2(\omega_1, \omega_2) &= \iint_{-\infty}^{\infty} p_2(x_1, x_2) e^{-j(\omega_1 x_1 + \omega_2 x_2)} dx_1 dx_2 \\ &= G(\omega_1, \omega_2, 0). \end{aligned} \quad (2)$$

For the general case of an orthonormally transformed coordinate system $\mathbf{t} = [t_1 \ t_2 \ t_3]^T$ of $\mathbf{x} = [x_1 \ x_2 \ x_3]^T$, where $\mathbf{t} = \mathbf{A}\mathbf{x}$ and $\Omega = \mathbf{A}\omega$, we have

$$\begin{aligned} P_1(\Omega_3) &= \int_{-\infty}^{\infty} p_1(t_3) e^{-j\Omega_3 t_3} dt_3 \\ &= G \left(\mathbf{A}^T \begin{bmatrix} 0 \\ 0 \\ \Omega_3 \end{bmatrix} \right), \end{aligned} \quad (3)$$

and

$$\begin{aligned} P_2(\Omega_1, \Omega_2) &= \iint_{-\infty}^{\infty} p_2(t_1, t_2) e^{-j(\Omega_1 t_1 + \Omega_2 t_2)} dt_1 dt_2 \\ &= G \left(\mathbf{A}^T \begin{bmatrix} \Omega_1 \\ \Omega_2 \\ 0 \end{bmatrix} \right). \end{aligned} \quad (4)$$

Thus, the Fourier transform of a linear/planar projection represents a linear trace/slice of the Fourier transform of the object itself. Given a complete set of projections, the entire Fourier space can be known. This is an important result that forms the basis for many image-reconstruction problems, for it shows that an image can be reconstructed from its projections through the use of the inverse Fourier transform.

4. HOW THE DATA FITS INTO THE TOMOGRAPHIC FRAMEWORK

The Projection-Slice Theorem enables reconstructions of an object to be obtained from a complete set of projections. However, in a practical application, a complete set is difficult to obtain. In most cases, however, a good approximation is generally all that is desired. A separate problem is that true projections, or even accurate approximations, are difficult to obtain using laser sources such as this one, since the laser cannot penetrate a solid object such as a mine. The CCD images roughly approximate the integration of the reflectivity function of the mine and the water column, but cannot include obstructed areas of the scene. However, reconstructions

made from images such as these, while not ideal in any sense, still preserve the overall shape of the original objects [3]. The only registration that was performed on the CCD image data was to move the mine to the center of each image; each image was also scaled to a particular set of dimensions (8 meters by 8 meters). After these registrations were performed, the CCD images were treated as true 2D projections. The PMT returns do not resemble true 1D projections directly, and need to be processed accordingly before they can be treated as such. In particular, the section of the PMT returns following the initial water surface reflection follows the exponential form $\frac{e^{-2a\xi}}{(H+\xi/m)^2}$, where a represents the absorption coefficient of the ocean water, ξ represents the range in water, H is the altitude of the sensor, and m is the refraction index of water [4]. After compensating for the exponential character of the scattering in the water, the reflection pulse from the mine was clearly visible. However, the laser pulse used in this data set was too long to provide any meaningful information about the range dimensions of the mine. The reason is that the radius of the mine (.5 meter) was too small compared to the length of the laser pulse (6 ns translates to 1.35 meters per pulse in water). The pulse also widens due to scattering after reflection off the mine. As a result, the PMT returns, while extremely valuable in the detection process, are of little value at present for our tomographic efforts with this data set.

5. ALGORITHM

The first step in the reconstruction algorithm is the registration of the CCD images; each image is circularly shifted so that the mine appears centered, and each is dimensionally scaled to represent the same area. At this point, each image is treated as a true 2D projection, and the next step is to calculate the correct rotation matrix \mathbf{A} based on the location of the mine and sensors, as well as the direction of propagation of the laser. Locations of all relevant objects are given by aircraft instruments and GPS data in terms of relative East (treated as x_1), North (x_2), and Z (x_3) coordinates, where Z represents altitude with respect to sea level. We defined \mathbf{A} in terms of two angles θ and ϕ ; we define θ as the angle between the direction of propagation of the laser in water (considered t_3) and the x_3 -axis, while ϕ is defined as the angle between the x_1 -axis and the projection of t_3 onto the x_1x_2 -plane. Thus, θ and ϕ are rotation angles relating the line of sight (t_3) to the principle coordinate axes. At this point, the Projection-Slice Theorem is applied; the Fourier transform of each projection corresponds to a slice of the Fourier transform of the reflectivity function of the scatterers in the water column taken at the same angles θ and ϕ . The Projection-Slice Theorem can be easily shown to hold for discrete time/space signals using the discrete time Fourier transform (DTFT). We use the fast Fourier transform (FFT) to sample the DTFT of each CCD image; thus, we obtain Fourier data along the dimensions Ω_1 and Ω_2 corresponding to the discrete-valued coordinate system \mathbf{t} , which are related to the discrete Fourier dimensions ω corresponding to the discrete valued coordinate system \mathbf{x} by

$$\begin{bmatrix} \omega_1 \\ \omega_2 \\ \omega_3 \end{bmatrix} = \mathbf{A}^T \begin{bmatrix} \Omega_1 \\ \Omega_2 \\ 0 \end{bmatrix},$$

as described in Section 3. Each set of Fourier data, however, must be resampled onto a Cartesian grid so that the Fourier domain data can be inverted back to the spatial domain using a fast algorithm.

This resampling is done with a simple nearest-neighbor interpolation. Finally, after the Fourier data from each image has been incorporated into the Cartesian grid, the reconstruction is completed by taking its inverse FFT.

6. EXPERIMENTAL RESULTS

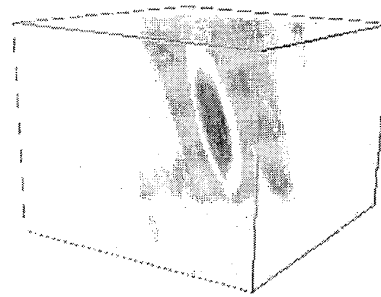
The results for the reconstruction from the CEFT data are shown in Fig. 1(a). Notice that instead of a sphere appearing in the center of the volume, we see an off-axis ellipsoid. The object appears off-axis and ellipsoidal because the look angles had diversity in ϕ of only around 60 degrees and only ranged from 13 to 18 degrees in θ . For a fixed θ , an increase in ϕ -diversity tends to cause a reconstruction of a spherical object to become less elongated and more on line with the x_3 -axis, as experiments with analytical projections show. Of course, the best reconstructions of objects of this nature using fixed θ are achieved with $\theta = 90$ degrees. To judge the quality of our reconstruction from CEFT data, a reconstruction was performed using theoretical projections from a sphere taken at exactly the same angles as the real data. This reconstruction, shown in Fig. 1(b), closely resembles the off-axis ellipsoid found in the CEFT reconstruction. In addition, planar slices of each reconstruction are shown in Fig. 2 and Fig. 3, respectively. Note that the shape and angular orientation of the reconstructed mine in each planar slice is similar to that of the object reconstructed from analytical projections. This shows that our modeling of the CCD images as true projections was not unjustified, and suggests that a richer dataset with greater angular diversity should greatly improve the quality of reconstructions.

7. CONCLUSION

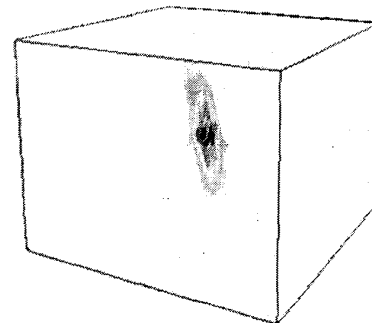
In this paper, we have extended the use of data collected for a mine detection system into a tomographic imaging problem. We have taken CCD images and PMT data from a system designed solely for detection and used them in a tomographic framework, and produced results which, while not ideal, suggest that a system designed for the tomographic imaging problem could produce high-quality reconstructions. The limits on the quality of results achieved in this paper are attributed to the lack of a rich dataset with a wide range of look angles, as well as a pulse width too wide for meaningful PMT data. Since our reconstruction from real data was similar to the reconstruction from theoretical projections, these preliminary results are promising for future experiments, especially if some form of pre-processing is performed on a complete dataset so that the data more closely resemble true projections. Finally, better time resolved data, such as PMT returns from a shorter or modulated laser pulse, should improve reconstruction quality along the range direction.

8. REFERENCES

- [1] F. Natterer, *The Mathematics of Computerized Tomography*, John Wiley & Sons, New York, 1986.
- [2] Dan E. Dudgeon and Russell M. Mersereau, *Multidimensional Digital Signal Processing*, Prentice Hall, Englewood Cliffs, NJ, 1984.
- [3] A.J. Johnson, D.L. Marks, R.A. Stack, D.J. Brady, and D.C. Munson, Jr., "Three-dimensional surface reconstruction of optical lambertian objects using cone-beam tomography," in



a)

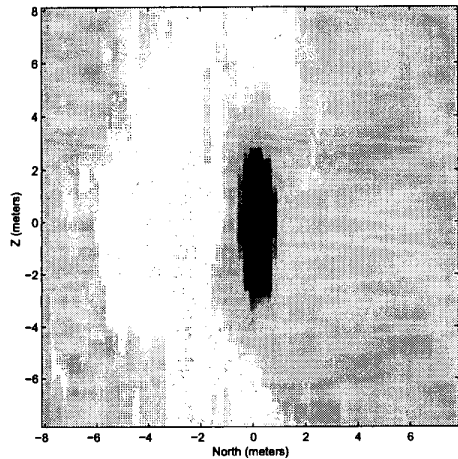


b)

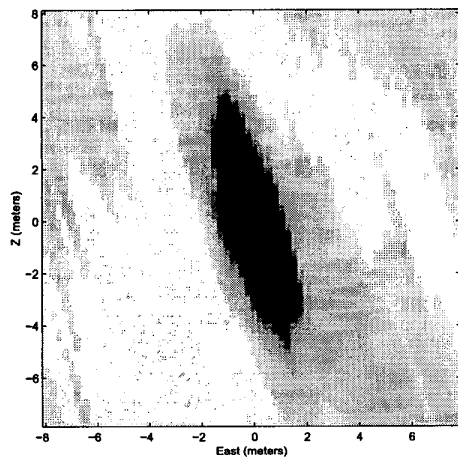
Fig. 1. a) 3D rendering of reconstruction from CEFT data. b) 3D rendering from analytical projections.

Proceedings of 1999 International Conference on Image Processing, 1999, pp. 663-7 vol.2.

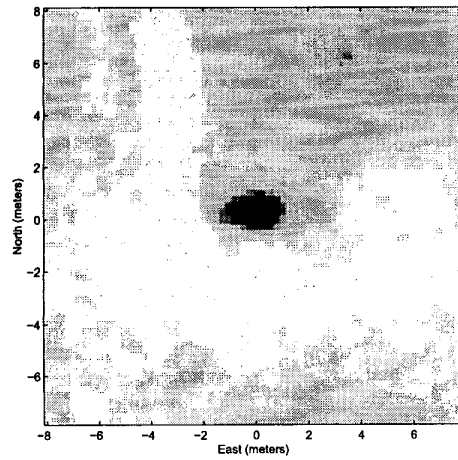
- [4] Ronald E. Walker, *Marine Light Field Statistics*, John Wiley & Sons, New York, 1994.
- [5] Charles V. Jakowatz, Jr., Daniel E. Wahl, et al., *Spotlight-Mode Synthetic Aperture Radar: A Signal Processing Approach*, Kluwer Academic Publishers, Boston, 1996.
- [6] Russell M. Mersereau and Alan V. Oppenheim, "Digital reconstruction of multidimensional signals from their projections," *Proceedings of the IEEE*, vol. 62, October 1974.



a)

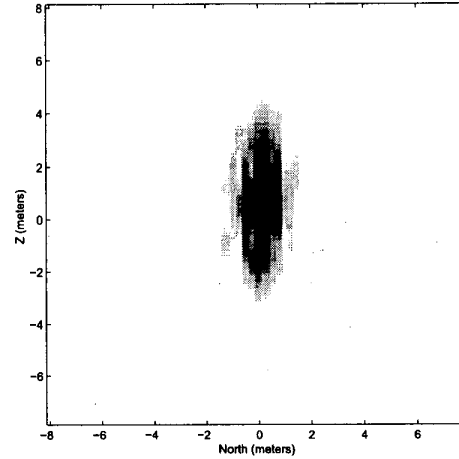


b)

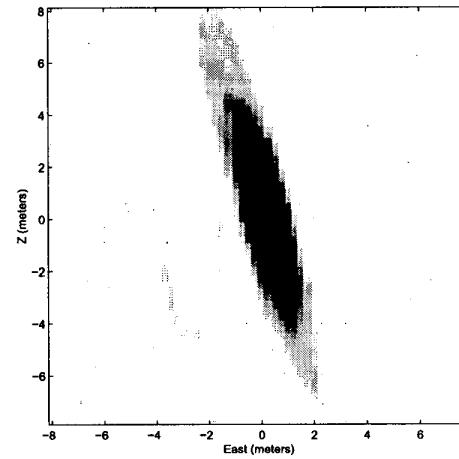


c)

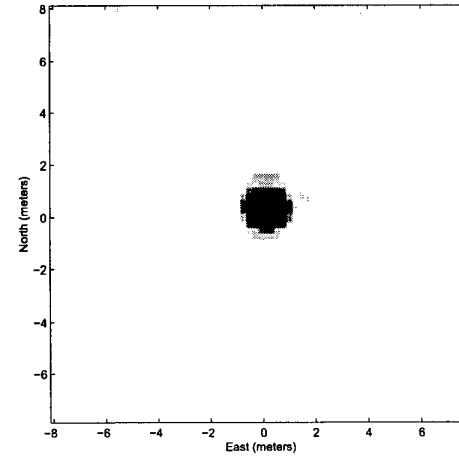
Fig. 2. Planar slices of reconstructed mine from CEFT data. a) North-Z plane. b) East-Z plane. c) East-North plane.



a)



b)



c)

Fig. 3. Slices of mine reconstruction from analytical projections. a) North-Z plane. b) East-Z plane. c) East-North plane.